Rotationally resolved electronic spectroscopy of biomolecules in the gas phase. Melatonin

John T. Yi [a,1], Christian Brand [b,1], Miriam Wollenhaupt [b], David W. Pratt [a], W. Leo Meerts [c], Michael Schmitt [b,*]

[a] *University of Pittsburgh, Department of Chemistry, Pittsburgh, PA 15260, USA*
[b] *Heinrich-Heine-Universität, Institut für Physikalische Chemie I, 40225 Düsseldorf, Germany*
[c] *Radboud University Nijmegen, Institute for Molecules and Materials, Heyendaalseweg 135, NL-6525 AJ Nijmegen, The Netherlands*

ARTICLE INFO

ABSTRACT

Rotationally resolved electronic spectra of the A and B bands of melatonin have been analyzed using an evolutionary strategy approach. From a comparison of the *ab initio* calculated structures of energy selected conformers to the experimental rotational constants, the A band could be shown to be due to a gauche structure of the side chain, while the B band is an anti structure. Both bands show a complicated pattern due to a splitting from the threefold internal rotation of the methyl rotor in the N-acetyl group of the molecules. From a torsional analysis we additionally were able to determine the barriers of the methyl torsion in both electronic states of melatonin B and give an estimate for the change of the barrier upon electronic excitation in melatonin A. The electronic nature of the lowest excited singlet state could be determined to be ^1L_b (as in the chromophore indole) from comparison to the results of *ab initio* calculations.

1. Introduction

Melatonin (N-acetyl-5-methoxytryptamine) is an animal and plant hormone [1] which regulates physiological processes like the circadian rhythms [2], influences the immune system [3], and acts as free radical scavenger and potent antioxidant [4]. Its physiological action strongly depends on the interaction with specific receptors. Quantitative structure–activity relationship (QSAR) studies have proven that the crucial motifs for pharmacological activity are the methoxy and the N-acetyl groups, while indole merely serves as scaffold which determines the distance and relative orientation of these groups. Even the chemically very different naphthalene [5] or tetrahydronaphthalene molecules [6] are good bioisosteric substitutes for indole in melatonin analogs. The exact knowledge of the conformer space of these biologically active serotonin derivatives is crucial for performing and understanding experiments on structure–affinity relationships.

Dian et al. [7] studied the infrared-induced conformational isomerization and vibrational relaxation dynamics in melatonin using IR–UV hole-filling spectroscopy and IR-induced population transfer spectroscopy. Using a combination of two-color resonant two-photon ionization (R2PI), laser-induced fluorescence (LIF), resonant ion-dip infrared spectroscopy (RIDIRS), fluorescence-dip infrared spectroscopy (FDIRS), and UV–UV hole-burning spectroscopy, Florio et al. [8] investigated the conformational preferences of melatonin in a molecular beam. They identified three major *trans*-amide conformers and two minor *cis*-amide structures. Florio and Zwier [9] studied the influence of water solvation on the conformational space of melatonin. Contrary to the case of tryptamine [10], the conformational richness is not significantly influenced by water complexation. The gas phase He(I) photoelectron spectra of melatonin have been reported by Kubota and Kobayashi [11]. They found that the interaction of the π orbital of the 5-methoxyindole part of the molecule and the π and the $n_{C=O}$ orbitals of the N-ethylacetamide moiety depend strongly on the conformations.

In the present work, we investigate two major conformers of melatonin by a combination of rotationally resolved electronic spectroscopy and *ab initio* calculations. In molecules of this size, the rotational constants are relatively small, so that the classical line position assignment of the spectra seems to be reaching its limits here. Up to 100 single rovibronic transitions with intensities of more than 10% of the strongest line can contribute to one feature which is observed as "line" in the experimental rovibronic spectrum. As a result, semi-automated procedures that rely on evolutionary strategies have been used to fit these spectra, thereby testing the applicability of this approach to even larger systems.

* Corresponding author. Fax: +49 211 81 15195.
  E-mail addresses: pratt@pitt.edu (D.W. Pratt), leo.meerts@science.ru.nl (W. Leo Meerts), mschmitt@uni-duesseldorf.de (M. Schmitt).
[1] These authors contributed equally to the present publication.

2. Experimental details

The experiments were performed at the University of Pittsburgh, using an experimental setup that have been described elsewhere [12]. In brief, melatonin was heated to 175–225 °C, seeded in 300–500 mbar of argon, and expanded into vacuum. The beam was confined by skimmers, resulting in Doppler-broadening of individual rotational lines to 20 MHz full-width-at-half-maximum (FWHM) in a differentially pumped vacuum system. The molecular beam was crossed at right angles by UV radiation near 280 nm using an Ar⁺-pumped frequency doubled ring dye laser (FWHM < 1 MHz, Spectra Physics 380D). The integrated laser-induced fluorescence was collected using a lens system and detected by a photomultiplier tube. The relative frequency was determined to ±0.0005 MHz by comparison to a quasi-confocal Fabry–Perot interferometer and the absolute frequency was determined by simultaneously recording the iodine absorption spectrum and successive comparison to the tabulated transition frequencies [13].

3. Computational details

3.1. Ab initio calculations

Structure optimizations were performed employing the valence triple-zeta basis set with polarization functions (d, p) from the TURBOMOLE library [14,15]. The equilibrium geometries of the electronic ground and the lowest excited singlet states were optimized using the approximate coupled cluster singles and doubles model (CC2) employing the resolution-of-the-identity approximation (RI) [16–18].

Singlet state energies and wavefunctions were calculated using the combined density functional theory/multi-reference configuration interaction (DFT/MRCI) method developed by Grimme and Waletzke [19]. Configuration state functions (CSFs) in the MRCI expansion were constructed from Kohn–Sham (KS) orbitals, optimized for the dominant closed shell determinant of the electronic ground state employing the BH-LYP [20,21] functional. All 56 valence electrons were correlated in the MRCI runs and the eigenvalues and eigenvectors of five singlet states were determined. The *initial* set of reference configuration state functions was generated automatically in a complete active space type procedure (including all single and double excitations from the five highest occupied molecular orbitals in the KS determinant to the five lowest virtual orbitals) and was then iteratively improved. The MRCI expansion was kept moderate by extensive configuration selection. The selection of the most important CSFs is based on an energy gap criterion as described in Ref. [19]. Only those configurations were taken into account that have an energy below a certain cutoff energy. The energy of a given configuration was estimated from orbital energies within the selection procedure. The cutoff energy was given by the energy of the highest desired root as calculated for the reference space plus a cutoff parameter δE_{sel} = 1.0E_H. The latter choice has been shown to yield nearly converged results [19].

3.2. Evolution strategies used for spectra fitting

The rovibronic spectra were fit to a rigid asymmetric rotor Hamiltonian [22] by using a derandomized (DR) evolution strategy (ES) that was developed by Ostenmeier et al. [23]. A special implementation, which we employed in the present study, represents the second generation of derandomized ES and is abbreviated as DR2 [24]. It was shown [25] to be a very good alternative to the genetic algorithm based fits we have employed in the past [26]. Evolution strategies like DR2 are optimizers that are inspired by reproduction and natural selection in nature. While classical genetic algorithms aim to find a solution in the parameter space by ran-
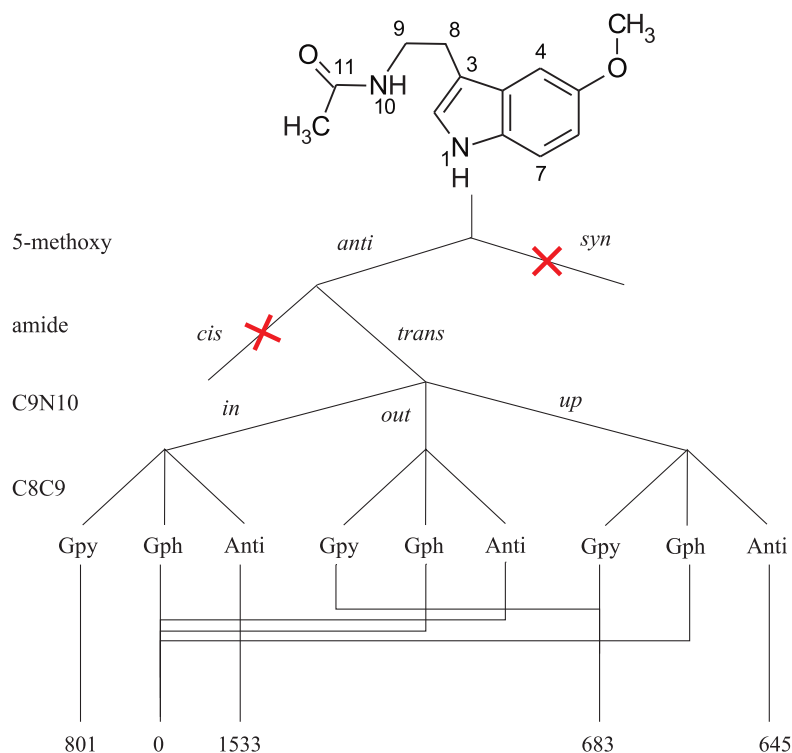
Fig. 1. Schematic overview of the tree of melatonin conformers. The *syn*-5-methoxy and the *cis*-amide branches have been discarded in this study. In the lower half, it is shown to which minimum the starting structures finally converge. At the bottom, the relative CC2 ground state energies (in cm⁻¹) of the CC2/cc-pVTZ optimized structures are given. For details see text.

Table 1
Relative CC2 ground state energies (in cm^{-1}) of the CC2/cc-pVTZ and CC2/TZVP optimized structures of various melatonin conformers. The energies are measured with respect to the most stable conformer at each level of theory. Rotational constants (in MHz) in both electronic states are for the CC2/cc-pVTZ optimized structures. Adiabatic CC2 excitation energies v_0 at CC2/cc-pVTZ optimized structures in cm^{-1} without ZPE correction.

Conformer	Relative CC2 energy		S_0			S_1			v_0
	cc-pVTZ	TZVP	A	B	C	ΔA	ΔB	ΔC	
Gph(trans-in)/anti	0	0	550	497	309	+10	+10	+15	33 931
Anti(trans-out)/anti	645	934	630	339	226	+1	+2	+1	34 091
Gpy(trans-out)/ anti	683	593	544	505	305	+42	−4	+21	33 680
Gpy(trans-in)/anti	801	648	785	310	266	+3	−10	−10	34 317
Anti(trans-in)/anti	1533	1925	775	230	181	−4	0	+1	34 440

domly combining information from a set of trial solutions, the DR2 algorithm can sense in which direction the quality of a fit increases. In the first step, the DR2 algorithm generates trial solutions (offspring) by using a random distribution around some starting point (parent) each consisting of the complete parameter set which is necessary to simulate the spectrum. Offspring with higher fitness than the parent are kept and used to compute the next generation. The DR2 algorithm makes use of the parameter correlation matrix for successive changes in the parents (mutations). This means that if for some parameter a parent has evolved in the same direction for several generations, resulting in a positive correlation, the most likely solution is assumed to be further in that direction and the next parameter mutation will be larger. Correspondingly, two anticorrelated mutations will lead to a smaller mutation. Compared to classical genetic algorithms, this procedure has been shown to lead to faster convergence of the parameters [25].

4. Theoretical results

4.1. Conformer structures and energies

The nomenclature for the melatonin conformers follows the suggestion of Florio et al. [8]. In their study, they optimized different melatonin conformers, which have been preselected via OPLS-AA force field calculations, using density functional theory with the Becke-3LYP functional and the 6-31+G*(5d) basis set. The electronic energies of the lowest energy conformers were determined via single-point localized MP2/aug-cc-pVTZ(-f) calculations and corrected for zero-point vibrational contributions using the Becke-3LYP/6-31+G*(5d) vibrational frequencies.

We decided to follow another route for determination of the geometries at the minima of the potential energy surface and the respective energies. Structure optimizations were performed with the approximate coupled cluster singles and doubles model (CC2) within the resolution-of-the-identity approximation (RI) using the cc-pVTZ basis set. This combination of method and basis set has been shown to yield very good results for the structures in the electronic ground and excited singlet states, measured by the differences between the observed rotational constants and the calculated ones. At these geometries, the ground state and excitation energies have been calculated using the DFT/MRCI method from Grimme and Waletzke [19].

Due to the expensive method and the large conformational space, we restricted our search considerably to a subspace that was chosen from experiences on similar systems. Only these starting structures were then subjected to geometry optimization at the CC2/cc-pVTZ level of theory. Melatonin has the following degrees of freedom for internal motions that have to be considered in the generation of the conformers; a threefold rotation about the C8—C9 bond, resulting in two different *gauche* and one *anti* conformations, a twofold rotation about the amide bond (N10—C11)), which generates *cis*- or *trans*-amide structures, and a twofold rotation of the 5-methoxy group, which can lead to *syn* and *anti*

conformers, *cf.* Fig. 1. From the analysis of the rotationally resolved spectra of 5-methoxyindole [27] and 5-methoxytryptamine [28], we have learned that all experimentally observed conformers belonged to the *anti* class of conformers for the methoxy group with respect to the indole NH. Therefore, we excluded from the beginning all *syn*-methoxy conformers. Since the *cis*-amide conformers are considerably higher in energy than the respective *trans*-amide structures, they also were not considered as starting structures. Thus, three classes of conformers served as basis of the conformational search; the first is based on the Anti(trans)anti family, the second on the Gpy(trans)anti, and the third on the Gph(trans)anti structures. The remaining degree of freedom is the threefold rotation about the C9—N10 bond, which leads to conformers that are labeled by the orientation of the amide N—H with respect to the chromophore as *in*, *out*, and *up*.

For the Anti(trans)anti family the *in*, *out*, and *up* conformers have been used as starting structures, resulting in Anti(trans-out)/anti and Anti(trans-in)/anti minima on the potential energy surface. The *up* structure converged in the course of the optimization to the Anti(trans-in)/anti minimum. Also, for the two Gauche families, the *up* conformer converged to one of the *in* and *out* conformers. For the Gph conformers, additionally, the *out* conformer relaxed to the *in* structure. Thus, five low energy conformers of melatonin are found in our analysis, keeping in mind that we did not explore the whole conformational space.

Table 1 shows the energies, relative stabilities and rotational constants of the five lowest energy conformers of melatonin found in our study, calculated for the CC2/cc-pVTZ optimized structures. The most stable conformer was found to be Gph(trans-in)anti, followed by *Anti(trans-out)/anti*, 645 cm^{-1} above. The energetically following conformer is the analog of the most stable, but with the side chain pointing in the pyrrole direction *Gpy(trans-in)anti*, 683 cm^{-1} above the minimum. In order to check how much the energetics are influenced by BSSE effects of the side chain–chromophore interaction, we optimized the structures of the three most stable conformers with the smaller TZVP basis. The relative energy of the *Anti(trans-out)/anti* conformer increases, while *Gpy(trans-in)anti* and Gph(trans-in)anti stay constant relative to each other. Obviously, BSSE effects stabilize both gauche structures equally and will not cause large variations in their relative energies.

The adiabatic excitation energy (CC2/cc-pVTZ) of the Anti (trans-out)/anti conformer is calculated to be 34 091 cm^{-1} for

Table 2
Adiabatic DFT/MRCI excitation energies v_0 of the lowest excited singlet state at CC2/cc-pVTZ optimized structures in cm^{-1} without ZPE correction. θ and ϕ are the polar angles of the TDM in the inertial axis system of the respective conformer, and θ^{ref} is the angle of the TDM with the *a*-axis (the *pseudo*-symmetry axis) in the indole chromophore, cf. Fig. 2.

Conformer	v_0	θ	ϕ	θ^{ref}	f
Gph(trans-in)/anti	34 108	16	67	53	0.07
Anti(trans-out)/anti	33 797	−22	82	51	0.08
Gpy(trans-out)/anti	33 410	−40	65	52	0.07
Gpy(trans-in)/anti	33 824	−142	66	46	0.07
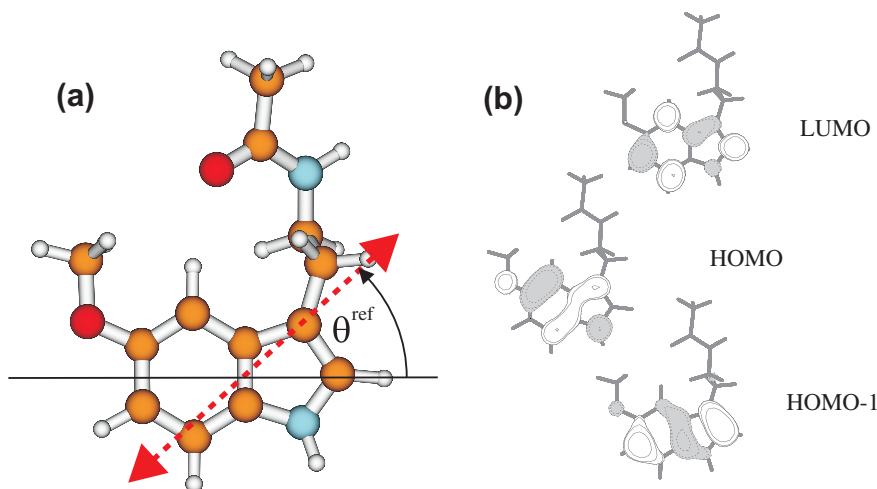
Fig. 2. (a) Definition of θ^{ref}, the angle between the TDM and the *pseudo*-symmetry axis of the indole chromophore. (b) Frontier orbitals of the Anti(trans-out)/anti conformer.

Gph(trans-in)anti 33 931 cm^{-1}, and for Gpy(trans-in)anti 34 317 cm^{-1}. The differences of the excitation energies are considerably larger than the wavenumber difference of the origin bands of conformers A–E in Ref. [8]. In order to quantify the excitation properties, we calculated excitation energies and transition dipole moments using DFT/MRCI at the CC2 optimized structures. This is described in the following section.

4.2. Excited singlet states

Using DFT/MRCI at the CC2 optimized geometries, we calculated excitation properties of the four lowest energy conformers, described in the preceding section. Table 2 gives the lowest adiabatic singlet excitation energies of the four lowest energy conformers along with the orientations of the transition dipole moments

(TDM) in the principal inertial axis system of the conformers (θ and ϕ), and also with respect to the *pseudo*-symmetry axis of the indole chromophore (θ^{ref}, cf. Fig. 2a), which is independent of the different inertial axis orientations in the different conformers. The lowest singlet excitation of all four conformers has its TDM oriented as in the ^1L_b state of indole, with slightly larger angles θ^{ref} than in indole (+38.3°). The positive direction of the angle θ^{ref} is defined in Fig. 2a.

The excitation scheme of the lowest singlet excitation is that of a nearly pure LUMO ← HOMO transition (*cf.* Fig. 2b). The excitation to the second singlet state, which is the ^1L_a-state, is mainly of LUMO ← HOMO − 1 character. These excitation schemes for the ^1L_a and ^1L_b states are different than those of indole. As we showed in a recent publication on 5-methoxyindole [27], the methoxy substituent introduces an additional node in the molecular orbital, which
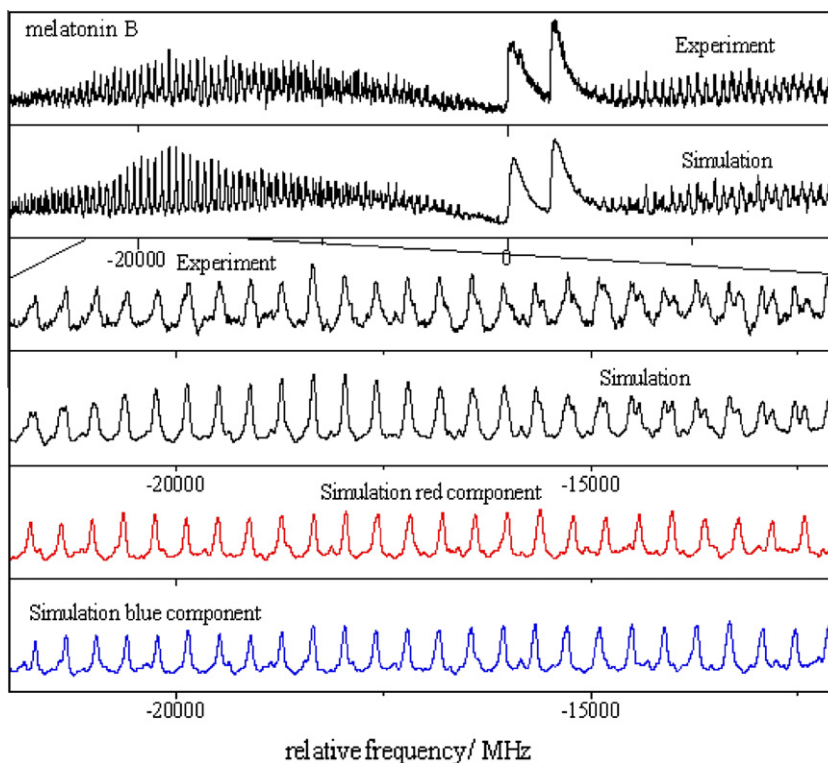
Fig. 3. Experimental and simulated spectrum of melatonin B. The lower four traces show expanded views of the experiment, the simulation and the deconvolution into the two torsional subbands. For details see text.
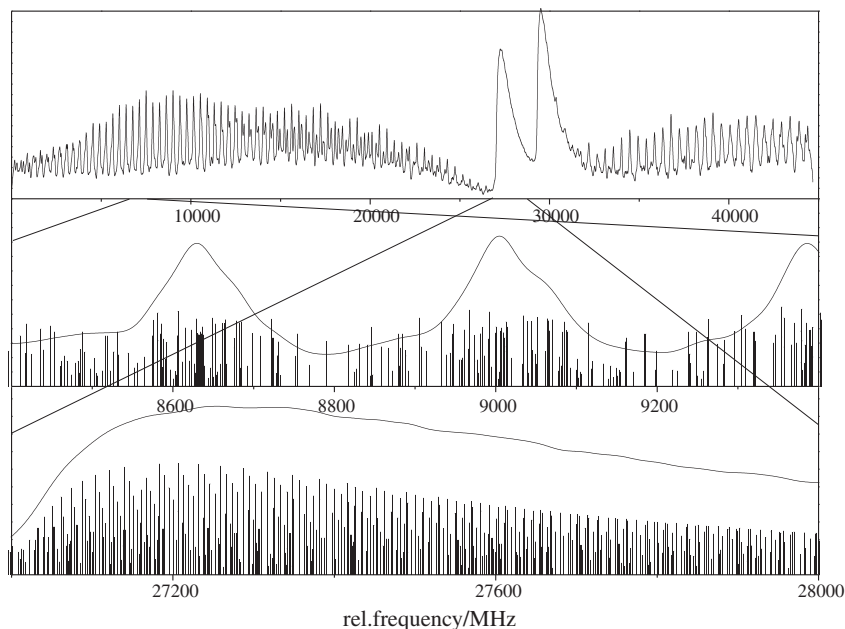
Fig. 4. Simulated stick spectrum of melatonin B along with the convolution, using the experimental line width. The lower two traces show enlarged regions of the spectra in the *P*- and in the *Q*-branch, illustrating the complexity of the spectrum at this resolution.

was formerly the HOMO − 1 in indole, and which becomes the HOMO in 5-methoxyindole. This causes a change in energy ordering between indole, 5-methoxyindole and melatonin for the HOMO and HOMO − 1, respectively, and is responsible for the altered excitation scheme of melatonin compared to indole.

The second excited singlet state is the ^1L_a state, about 4000 cm^{-1} above the ^1L_b state for each conformer, with an oscillator strength of about 0.14 (approximately twice that of the ^1L_b state). The permanent dipole moment of this state is calculated to be more than twice that of the ^1L_b state (7.4 vs. 3.5 Debye).

5. Experimental results

The rotationally resolved LIF spectrum of melatonin B (referring to the nomenclature of Florio et al. [8]) shows a split band with Δv of 2270 MHz, *cf.* Fig. 3. The fit of the spectrum shows that both subbands have very similar rotational constants, both in the ground and in the electronically excited states. The lower frequency component can be fit with a normal rigid rotor Hamiltonian, while the blue component shows slight deviations. We based the analysis of the structure of this conformer on the rotational constants of the red component.

The need for using the automated evolution fitting procedure described above is illustrated in Fig. 4. Two different regions of the simulated spectrum have been enlarged in the figure in order to highlight the enormous number of rovibronic transitions that contribute to the observable features, which appear as single lines in the spectrum. In the outer wings of the *P*-branch, up to 100 lines contribute to each feature; in the region of the *Q*-branch it is a few hundred. A quantum-number based assignment procedure as has been used in the analysis of smaller molecules for decades is thus impossible here.

Comparison to the results of *ab initio* calculations (CC2/cc-pVTZ) proves that only the rotational constants of the Anti(trans-out)/ anti conformer are in agreement with the experimental ones (*cf.* Fig. 5). The splitting has to be assigned to a large amplitude motion. Here, we have two possible ones; the threefold methyl rotation of the 5-methoxy group (high barrier) and the threefold methyl

rotation of the acetyl group (low barrier). N-phenylacetamide for example, has a ground state barrier for the methyl rotation in the acetyl group of less than 30 cm^{-1}, and of 50 cm^{-1} in the electronically excited state with an experimentally observed AE splitting of about 4 cm^{-1} [29]. In melatonin, the acetamide group is separated from the chromophore by two methylene groups. Therefore, we expect the torsional barrier of the methyl group to be similar in both electronic states, resulting in a much smaller AE splitting. The chemically more similar N-phenethyl-acetamide shows no observable AE splitting of the origin band in the R2PI spectrum [30].

We fit both subbands in the rotational spectrum of melatonin B to an effective rotational Hamiltonian for the torsional state $|v,\sigma\rangle$, which is defined as [31,32]:
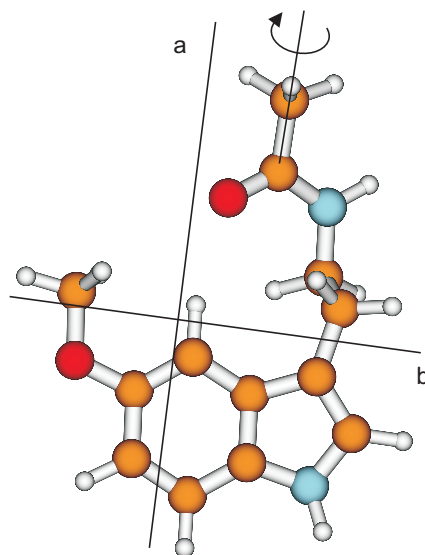
Fig. 5. Inertial *a* and *b*-axes of the Anti(trans-out)/anti conformer of melatonin along with the internal rotor axis of the methyl rotor in the acetyl group. The internal rotor axis is nearly parallel with respect to the inertial *a*-axis.
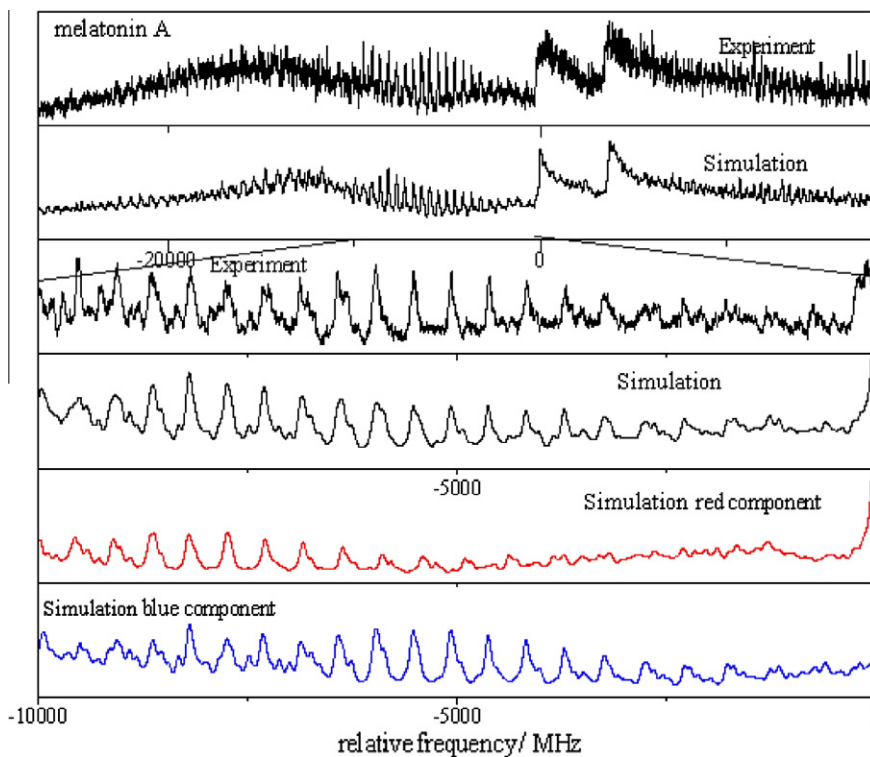
Fig. 6. Experimental and simulated spectrum of melatonin A. The lower four traces show expanded views of the experiment, the simulation and the deconvolution into the two torsional subbands. For details see text.

$$H_R^{v\sigma} = \sum_{g=a,b,c} B_g^{v\sigma} P_g^2 + \sum_{g=a,b,c} D_g P_g \qquad (1)$$

The quantum-numbers, v and σ, are introduced to unambiguously classify the energy levels for the torsional problem. v is the principal torsional quantum-number used to classify the torsional states for a single threefold potential and the three torsional sublevels have to be distinguished by a further quantum-number σ. This σ is chosen in such a way that it represents the symmetry of the torsional wavefunctions and therefore the torsional problem is diagonal in σ. The $B_g^{v\sigma}$ are the torsionally averaged rotational constants for the state $|v,\sigma\rangle$ (terms quadratic in the overall angular momenta P_g), and the terms linear in angular momentum D_g are defined by

$$D_g = \frac{\lambda_g B_g W_{v\sigma}^{(1)}}{r} \qquad (2)$$

From the *ab initio* calculated structure of Anti(trans-out)/anti melatonin, we know that the methyl rotor of the acetyl group is parallel to the inertial a-axis and perpendicular to b and c (cf. Fig. 5). Therefore, only one linear term, namely D_a is needed, while D_b and D_c are zero. λ_g are the direction cosines of the methyl top axis and the main inertial axes (in the case at hand, $\lambda_a = 1$, $\lambda_b = \lambda_c = 0$). $W_{v\sigma}^{(1)}$ the first order perturbation coefficient for the state $|v,\sigma\rangle$, is given by

$$W_{v\sigma}^{(1)} = -2\langle v\sigma|p|v\sigma\rangle \qquad (3)$$

and

$$r = 1 - \sum_{g=a,b,c} \frac{\lambda_g^2 I_\alpha}{I_g} \qquad (4)$$

where I_α is the moment of inertia of the methyl top and I_g are the moments of inertia of the whole molecule with respect to the main inertial axes. The $B_g^{v\sigma}$ are defined by

$$B_g^{v\sigma} = B_g + F W_{v\sigma}^{(2)} \qquad (5)$$

with second order perturbation coefficients $W_{v\sigma}^{(2)}$ given by

$$W_{v\sigma}^{(2)} = 1 + 4F \sum_{v' \neq v} \frac{|\langle v\sigma|p|v'\sigma\rangle|^2}{E_{v\sigma} - E_{v'\sigma}} \qquad (6)$$

Thus, the barrier to internal rotation and its change upon electronic excitation can be determined from the values of D_a, from the difference of the torsionally averaged rotational constants in the E and the A states, and from the subtorsional splitting $\Delta E_{ea} = (E_{v'\pm 1} - E_{v''\pm 1}) - (E_{v'0} - E_{v''0})$. Using a fitting program, which additionally uses the information of higher torsional transitions [33], we made a fit of the barriers in ground and excited state, including the $2e' \leftarrow 1e''$ transition, which we assigned to be the 41 cm^{-1} band in the low resolution R2PI spectrum of Florio et al. [8]. According to a harmonic normal mode analysis of Anti(trans-out)/anti melatonin, the lowest energy vibration is the bending vibration of the side chain at 87 cm^{-1}. It seems therefore safe to assign the lowest observed vibronic frequency to the torsional $2e' \leftarrow 1e''$ transition. Fixing the torsional constant F to 5.2 cm^{-1}, we obtained barriers of $V_3(S_0) = 63$ cm^{-1} and $V_3(S_1) = 64$ cm^{-1}. These values are larger than the ground state V_3 torsional barrier in acetamide that has been determined to be 25 cm^{-1} by microwave spectroscopy [34]. Also in this molecule, the inertial a-axis is nearly parallel to the internal rotor axis, as in melatonin B.

Since the methyl rotor points away from the bulky indole chromophore, the reason for the higher barrier in melatonin B compared to acetamide cannot be a steric one, but must be electronic. Plusquellic and Pratt [35] have shown that a correlation exists between the internal rotation barriers of methyl groups attached to a peptide bond and the relative weight of the two principal resonance structures (a purely covalent and an ionic resonance structure) that contribute to the peptide bond. The weight of these resonance structures strongly depends on the nature of the

Table 3

Molecular parameters of the melatonin A and B origin bands obtained from ES-DR2 fits of the experimental spectra. The changes of the rotational constants upon electronic excitation are defined as $\Delta A = A' - A''$, etc. where the doubly primed parameters refer to the electronic ground state and the singly primed to the excited state. The linear angular momentum terms D_a'' and D_a' are defined by Eq. (2). The angles θ and ϕ define the orientation of the transition dipole moment in the principal axis system of the molecule. θ is the angle between the projection vector of the transition dipole moment on the ab-plane, and the a-axis and ϕ the angle between the transition dipole moment and the c-axis. τ is the excited state lifetime, determined from the Lorentz contribution to the Voigt profile of the rovibronic transitions. T_1, T_1, and w_T are the parameters from a two-temperature fit [36] to the relative intensities of the rovibronic transitions: $n(T_1, T_2, w_T) = e^{-E/kT_1} + w_T e^{-E/kT_2}$.

	Anti(trans-out)anti		Gph(trans-in)anti	
	A	E	A	E
A'' (MHz)	627.62(7)	627.30(7)	541.99(22)	543.93(19)
B'' (MHz)	327.50(4)	327.50	487.03(17)	488.90(14)
C'' (MHz)	221.41(4)	221.41	312.26(13)	311.70(12)
D_a'' (MHz)	–	338.7(10)	–	–
$\Delta I''$ (uA^2)	−65.8(2)	−66.2(2)	−351.9(1)	−341.6(1)
ΔA (MHz)	0.80(3)	0.73(3)	0.62(1)	0.57(2)
ΔB (MHz)	1.12(8)	1.12(7)	8.19(2)	7.53(5)
ΔC (MHz)	0.67(2)	0.76(2)	7.55(3)	6.64(3)
$\Delta I'$ (uA^2)	−66.1(2)	−66.5(2)	−371.9(1)	−358.7(1)
D_a' (MHz)	–	326.8(11)	–	–
θ (degree)	39	39	25	25
ϕ (degree)	88	88	81	81
τ (ns)	3	3	2	2
T_1	9.7	9.7	4.5	4.5
T_2	2.7	2.7	13.4	13.4
w_T	0.34	0.34	0.08	0.08
v_0 (cm^{-1})	32549.19(1)	32549.11(1)	32978.04(1)	32977.92
ΔE_{ea} (MHz)	−2262(3)		−3640(20)	
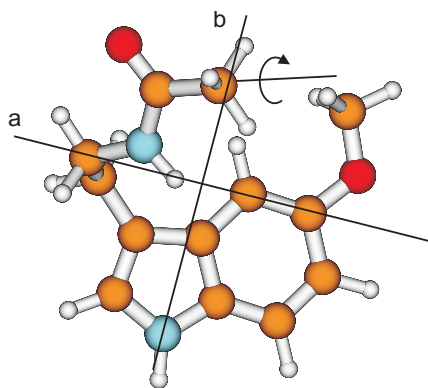
Fig. 7. Inertial a and b-axes of the Gph(trans-in)/anti conformer of melatonin along with the internal rotor axis of the methyl rotor in the acetyl group. The polar angles of the internal rotor axis with the inertial axes are $\zeta = 40°$ and $\eta = 10°$. Here η is the angle between the projection vector of the threefold rotor axis on the ab-plane and the a-axis and ζ the angle between the threefold rotor axis and the c-axis.

substituents at the peptide bond and their conformations. Thus, the difference of the melatonin B methyl rotor barrier compared to that of acetamide is easily understood.

The rotationally resolved electronic spectrum of the melatonin A band is shown in Fig. 6. Like the origin band of melatonin B, it is split into two torsional components, which are in this case 3640 MHz ($\sim$0.12 cm^{-1}) apart. Comparison of the rotational constants of the A subtorsional component, which are given in Table 3, to the results of the *ab initio* calculations shows good agreement with the rotational constants of the Gph(trans-in)anti conformer. Florio et al. [8] assigned the melatonin A band to belong to the *Gpy(trans-in)anti* conformer. Based on the energetics, the rotational constants and their changes upon electronic excitation (cf. Table 1),

we prefer the assignment of the melatonin A band being due to the Gph(trans-in)anti conformer, an alternative assignment which has not been explicitly excluded by Florio et al. [8].

The center frequency of the melatonin A band is found at 32 978.04 cm^{-1}, thus 430 cm^{-1} blue-shifted relative to the origin of melatonin B, which could unambiguously be attributed to the Anti(trans-out)anti conformer. Comparing the DFT/MRCI computed origin frequencies from Table 2, one finds the origin of melatonin Gph(trans-in)anti to be blue-shifted by 311 cm^{-1}, while the origins of both Gpy conformers are red-shifted. This is a further indication that our assignment of melatonin A to the Gph(trans-in)anti conformer is correct.

The torsional analysis in this case is much more difficult than in the case of melatonin B, since the torsional axis makes an angle with all three inertial axes (cf. Fig. 7). Thus, in addition to the rotational constants for the A and the E subspectra, all three D_g have to be fit for each electronic state. This proved to be impossible for this conformer owing to the enormous line density of overlapping transitions. Using the subtorsional splitting of 3640 MHz and a frequency of 45 cm^{-1} for the $2e' \leftarrow 1e''$ transition of this conformer from Ref. [8], we could estimate the difference of the torsional barriers upon electronic excitation to about 6 cm^{-1} compared to 1 cm^{-1} for melatonin B.

6. Conclusions

Comparing the results of *ab initio calculations* with molecular parameters obtained from the analysis of the rotationally resolved electronic spectra of melatonin A and B, we were able to unambiguously assign a Gauche-phenyl structure to the melatonin A band, and an Anti-structure to melatonin B. The CC2/cc-pVTZ calculated ground state rotational constants of both conformers agree well with the experimentally determined ones. The changes of the rotational constants upon electronic excitation (and thus the excited state structure) are perfectly described by CC2 theory for melatonin B, while the calculated changes of the rotational constants ΔA and ΔC in melatonin A are slightly too large. This points to an overestimate of dispersive interactions at the CC2 level in the excited state of the folded melatonin A, while the linear melatonin B lacks dispersive interactions between side chain and chromophore and hence the geometry change upon electronic excitation is reproduced with higher accuracy for melatonin B. The spectra of both conformers are split by an internal threefold rotation of the methyl rotor in the acetyl group of the side chain. Since the spacing between the methyl rotor and the chromophore is large, and the side chain bearing the methyl group points away from the chromophore in the Anti-structure, the barriers in both electronic states are virtually the same. This situation changes in the Gauche-conformer. The electronic isolation of methyl top and chromophore is the same as in the Anti-conformer, but due to the close proximity of methyl rotor and chromophore, a through-space interaction may significantly change the barrier height upon electronic excitation.

Independent of the conformer, the lowest electronically excited singlet state has been found to be of ^1L_b character with nearly identical values of the transition dipole moment orientation with respect to the *pseudo*-symmetry axis of the indole chromophore.

conformers and Tim Zwier for sharing his geometry files for the starting structures of several melatonin conformers.

References

[1] M.M. Posmyk, K.M. Janas, Acta Physiol. Plant. 31 (2009) 1–11.
[2] J. Arendt, New Engl. J. Med. 343 (2010) 1114–1116.
[3] A. Carrillo-Vico, J.M. Guerrero, P.J. Lardone, R.J. Reiter, Endocrine 27 (2005) 189–200.
[4] D.X. Tan, L. Chen, B. Poeggeler, L. Manchester, R. Reiter, Endocr. J. 1 (1993) 57–60.
[5] M. Mathé-Allainmat, J. Andrieux, M. Langlois, Exp. Opin. Ther. Patents 7 (1997) 1447–1458.
[6] E. Fourmaintraux, P. Depreux, D. Lesieur, B. Guardiola-Lematre, C. Bennejean, P. Delagrange, H. Howell, Bioorgan. Med. Chem. 6 (1998) 9–13.
[7] B.C. Dian, G.M. Florio, J.R. Clarkson, A. Longarte, T.S. Zwier, J. Chem. Phys. 120 (2004) 9033–9047.
[8] G.M. Florio, R.A. Christie, K.D. Jordan, T.S. Zwier, J. Am. Chem. Soc. 124 (2002) 10236–10247.
[9] G.M. Florio, T.S. Zwier, J. Phys. Chem. A 107 (2003) 974–983.
[10] M. Schmitt, M. Böhm, C. Ratzer, C. Vu, I. Kalkman, W.L. Meerts, J. Am. Chem. Soc. 127 (2005) 10356–10364.
[11] M. Kubota, T. Kobayashi, J. Electron Spectrosc. Relat. Phenom. 128 (2003) 165–178.
[12] W.A. Majewski, J.F. Pfanstiel, D.F. Plusquellic, D.W. Pratt, in: A. Myers, T.R. Rizzo (Eds.), Laser Techniques in Chemistry; vol. 23 of Techniques of Chemistry Series, J. Wiley and Sons, 1995, p. 101.
[13] S. Gerstenkorn, P. Luc, Atlas du Spectre D'absorption de la Molécule D'iode 14 800–20 000 cm^{-1}, CNRS, Paris, 1986.
[14] R. Ahlrichs, M. Bär, M. Häser, H. Horn, C. Kölmel, Chem. Phys. Lett. 162 (1989) 165–169.
[15] A. Schäfer, C. Huber, R. Ahlrichs, J. Chem. Phys. 100 (1994) 5829–5835.
[16] C. Hättig, F. Weigend, J. Chem. Phys. 113 (2000) 5154–5161.
[17] C. Hättig, A. Köhn, J. Chem. Phys. 117 (2002) 6939–6951.
[18] C. Hättig, J. Chem. Phys. 118 (2002) 7751–7761.
[19] S. Grimme, M. Waletzke, J. Chem. Phys. 111 (1999) 5645–5655.
[20] A.D. Becke, J. Chem. Phys. 98 (1993) 1372–1377.
[21] C. Lee, W. Yang, R. Parr, Phys. Rev. B 37 (1988) 785–789.
[22] H.C. Allen, P.C. Cross, Molecular Vib-Rotors, Wiley, New York, 1963.
[23] A. Ostermeier, A. Gawelczyk, N. Hansen, Lecture Notes in Computer Science: Parallel Problem Solving from Nature (PPSN III), Springer, 1994, pp. 189–198.
[24] O.M. Shir, T. Bäck, in: Proceedings of the Genetic and Evolutionary Computation Conference, ACM Press, London, 2007; pp. 713–721.
[25] I. Kalkman, C. Vu, M. Schmitt, W.L. Meerts, ChemPhysChem 9 (2008) 1788–1797.
[26] W.L. Meerts, M. Schmitt, Int. Rev. Phys. Chem. 25 (2006) 353–406.
[27] C. Brand, O. Oeltermann, D.W. Pratt, R. Weinkauf, W.L. Meerts, W. van der Zande, K. Kleinermanns, M. Schmitt, J. Chem. Phys. 133 (2010) 024303-1–024303-11.
[28] T.B.C. Vu, I. Kalkman, W.L. Meerts, C. Brand, Y.N. Svartsov, S. Wiedemann, R. Weinkauf, M. Schmitt, Phys. Chem. Chem. Phys. 11 (2009) 2433–2440.
[29] S. Ullrich, K. Müller-Dethlefs, J. Phys. Chem. A 106 (2002) 9181–9187.
[30] V.A. Shubert, E.E. Baquero, J.R. Clarkson, J.A. Turk, A.A. Hare, K. Worrel, M.A. Lipton, D.P. Schofield, K.D. Jordan, T.S. Zwier, J. Chem. Phys. 127 (2007) (234315–1–234315, W.H.J. III).
[31] W. Gordy, R.L. Cook, Microwave Molecular Spectra, 3 ed., Wiley, New York, 1984.
[32] D.R. Herschbach, J. Chem. Phys. 31 (1959) 91–108.
[33] C. Jacoby, M. Schmitt, Chem. Phys. Chem. 5 (2004) 1686–1694.
[34] T. Kojima, E. Yano, K. Nakagawa, S. Tsunekawa, J. Mol. Spectrosc. 122 (1987) 408–416.
[35] D.F. Plusquellic, D.W. Pratt, J. Phys. Chem. A 111 (2007) 7391–7397.
[36] Y.R. Wu, D.H. Levy, J. Chem. Phys. 91 (1989) 5278–5284.